

# Experimental input from $e^+e^-$ for $a_\mu$ light-by-light

Y. P. Guo<sup>1\*</sup> on behalf of BESIII Collaboration

<sup>1</sup> Institut für Kernphysik, Johannes Gutenberg-Universität Mainz, Mainz, Germany

\* guo@uni-mainz.de

November 11, 2018



*Proceedings for the 15th International Workshop on Tau Lepton Physics,  
Amsterdam, The Netherlands, 24-28 September 2018*

scipost.org/SciPostPhysProc.Tau2018

## 1 Abstract

2 The anomalous magnetic momentum of the muon,  $a_\mu$ , has been measured and  
3 calculated with a precision up to 0.5 ppm, but there is a 3 to 4 standard  
4 deviations between these two values. The uncertainty in the calculation is  
5 dominated by the hadronic part, including the hadronic vacuum polarization  
6 and the hadronic light-by-light. The meson transition form factors and the  
7 helicity amplitudes can be used as input or constraint to the calculation of  
8 the hadronic light-by-light contribution. Latest experimental studies of the  
9 transition form factors of  $\pi^0$ ,  $\eta$ , and  $\eta'$  and the cross-section of  $\gamma\gamma^* \rightarrow \pi^+\pi^-$   
10 from  $e^+e^-$  collider are presented.

11

## 12 Contents

13	<b>1 Introduction</b>	<b>1</b>
14	<b>2 The BESIII experiment</b>	<b>2</b>
15	<b>3 Measurement at <math>e^+e^-</math> machine</b>	<b>3</b>
16	<b>4 Transition form factor measurement of pseudoscalar meson</b>	<b>3</b>
17	4.1 Space-like transition form factor measurements	4
18	4.2 Time-like transition form factor measurement of $\eta'$	6
19	<b>5 Measurement of <math>\gamma\gamma^* \rightarrow \pi^+\pi^-</math></b>	<b>7</b>
20	<b>6 Conclusion</b>	<b>8</b>
21	<b>References</b>	<b>8</b>

22

23

## 24 1 Introduction

25 The anomalous magnetic momentum of the muon,  $a_\mu \equiv (g-2)$ , has been considered as one  
26 of the observables with which the completeness of the Standard Model (SM) can be tested.

27 The direct measurement from the BNL experiment yields  $(11659208.9 \pm 6.3) \times 10^{-10}$ ,  
 28 with a statistical precision of 0.54 ppm [1]. The theoretical calculation in the SM has a  
 29 similar precision [2–4]. The difference between the measurement and the calculation is  
 30 3 to 4 standard deviations. A new experiment, started in 2017 at Fermilab [5], as well  
 31 as the planned experiment at J-PARC [6], aims to reduce the uncertainty of the direct  
 32 measurement by a factor of four; an improvement of the SM prediction is urgently needed.  
 33 The SM prediction contains the QED contribution, the weak contribution and the hadronic  
 34 contribution. The QED contribution is the largest one, it has been calculated up to 5-loop  
 35 in perturbation theory with a precision of 0.0007 ppm [7]. The weak contribution is small,  
 36 it has been calculated to 2-loop, with the measured Higgs mass taken into account [8],  
 37 and its uncertainty is well under control.

38 The hadronic contribution is the second largest one, but the largest to the uncertainty  
 39 of the SM calculation. It contains two components, the hadronic vacuum polarization  
 40 (HVP) contribution and the hadronic light-by-light (HLbL) contribution. Although the  
 41 absolute value of the HLbL is only 1.5% of the HVP, their uncertainties are at the same  
 42 level. Improvements from both are needed. The calculation of the HVP contribution  
 43 can be related to the hadronic cross-section via a dispersion relation, thus improving the  
 44 accuracy of the cross-section measurement can directly improve the precision of the HVP  
 45 calculation. While the situation for the HLbL part is different. So far, there are only  
 46 calculations from hadronic models. The validation of these models usually is done with  
 47 the meson transition form factor (TFF). Although different models use the same data  
 48 as constraint, the central values are different. Moreover, there is no reliable method to  
 49 estimate the uncertainty of these models. Recently, data-driven dispersive approaches  
 50 have been developed by two independent groups [9–16]. By using the meson TFF and the  
 51 helicity amplitudes of the two-photon cross-section as input, the dispersive approaches  
 52 build a direct relation between the HLbL contribution and experimentally measurable  
 53 variables. It allows a more precise prediction of both the central value and the uncer-  
 54 tainty. The dominant contribution from the HLbL comes from the pseudoscalar meson  
 55 exchange, followed by the meson loop contribution. These input variables can be mea-  
 56 sured in the time-like regime through the meson Dalitz decay process or radiative process  
 57 from  $e^+e^-$  annihilation, or in the space-like regime through two-photon fusion process at  
 58  $e^+e^-$  machine.

## 59 2 The BESIII experiment

60 The BESIII detector is a magnetic spectrometer [17] located at the Beijing Electron  
 61 Positron Collider (BEPCII). The cylindrical core of the BESIII detector consists of a  
 62 helium-based multilayer drift chamber (MDC), a plastic scintillator time-of-flight system  
 63 (TOF), and a CsI(Tl) electromagnetic calorimeter (EMC), all enclosed in a superconduct-  
 64 ing solenoidal magnet providing a 1.0 T magnetic field. The solenoid is supported by an  
 65 octagonal flux-return yoke with resistive plate counter muon identifier modules (MUC)  
 66 interleaved with steel. The acceptance of charged particles and photons is 93% over  $4\pi$   
 67 solid angle. The charged-particle momentum resolution at 1 GeV/ $c$  is 0.5%, and the  
 68  $dE/dx$  resolution is 6% for electrons from Bhabha scattering. The EMC measures photon  
 69 energies with a resolution of 2.5% (5%) at 1 GeV in the barrel (end cap) region. The  
 70 time resolution of the TOF barrel part is 68 ps, while that of the end cap is 110 ps. The  
 71 position resolution in MUC is about 2 cm.

72 The BEPCII is a  $\tau$ -charm factory, works with center-of-mass (CM) energy from 2.0  
 73 GeV to 4.6 GeV. The designed luminosity is  $1 \times 10^{33} \text{ cm}^{-2}\text{s}^{-1}$ . From 2009, the BESIII

74 experiment has collected large data samples at the full CM energies coverage region,  
 75 including  $5.9 \times 10^9$  events at the  $J/\psi$  peak,  $448.1 \times 10^6$  events at the  $\psi(2S)$  peak,  $2.9$   
 76  $\text{fb}^{-1}$  at the  $\psi(3770)$  peak, more than  $15 \text{fb}^{-1}$  at CM energies above 4.0 GeV, and a set of  
 77 data samples at 151 CM energies covers the whole energy region used for measurements  
 78 of  $R$ ,  $\tau$  physics, and baryon form factor measurement.

### 79 3 Measurement at $e^+e^-$ machine

80 The meson TFFs and helicity amplitude can be measured in space-like regime by using  
 81 the two-photon fusion process at  $e^+e^-$  machine or in time-like regime by using the Dalitz  
 82 decay process. Figure 1 shows the tree-level Feynman diagram for the two-photon process,  
 83 where  $q_1$  and  $q_2$  represents the momentum of the two photons emitted from the lepton  
 lines. Three techniques are used to study the two-photon process depending on the number

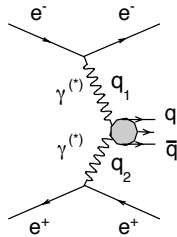


Figure 1: The Feynman diagram for the two-photon fusion process.

84 of leptons detected in the detector, namely, the untag, the single-tag, and the double-tag  
 85 method. In the untag case, only the hadronic productions is detected, the directions of  
 86 the leptons in the final state is required to parallel the beam direction. In this way, the  
 87 virtuality of both photons is very small ( $q_1^2, q_2^2 \simeq 0$ ), and can be considered as quasi-real.  
 88 In the single-tag case, one of the leptons is detected in the detector, while the other is  
 89 required to be scattered along the beam direction. In this case, the photon emitted from  
 90 the tagged lepton is far off-shell, while the untagged one is quasi-real. The TFF as a  
 91 function of  $Q^2$ ,  $F_{M\gamma^*\gamma^*}(q_1^2, q_2^2) \equiv F_{M\gamma^*\gamma}(Q^2)$  can be measured. In the double-tag case, all  
 92 the particles in the final state are detected, the TFF  $F_{M\gamma^*\gamma^*}(q_1^2, q_2^2)$  is accessible. This is  
 93 the input variable which can be used directly in the dispersive approaches. The double-  
 94 tag method is limited by statistics as the cross-section of the two-photon process strongly  
 95 peaks at small angle, so most of the current measurements are done with untag or single-  
 96 tag method. The studies presented here in space-like region are all performed in single-tag  
 97 method.  
 98 method.

### 99 4 Transition form factor measurement of pseudoscalar me- 100 son

101 The dominate contribution from the HLbL to  $a_\mu$  comes from the neutral pseudoscalar  
 102 exchange contribution,  $\pi^0$ ,  $\eta$ , and  $\eta'$  (see references from Ref. [2, 4]). Using a dispersive  
 103 approach, the pseudoscalar contribution to  $a_\mu^{\text{HLbL}}$  has been evaluated [23]. It can be  
 104 factorized as a two-dimensional integral of the universal weight functions times the form  
 105 factor dependent functions. The weight functions are model-independent. The study

106 shows that the region of photon momenta below 1.0 GeV (1.5 GeV) for  $\pi^0$  ( $\eta$  and  $\eta'$ )  
 107 gives the main contribution. The TFFs of these mesons in the space-like region have been  
 108 measured by the BaBar [18,19] and Belle [20] experiments recently, and in 1990s from the  
 109 CELLO [21] and CLEO [22] experiments. The results from these experiments are shown  
 110 in Fig. 2. The measurements from B-factories have high precision for  $Q^2 \geq 4 \text{ GeV}^2$ . The  
 111 CLEO measurement measures from  $Q^2 \geq 1.5 \text{ GeV}^2$ . In the region with  $Q^2 \leq 1.5 \text{ GeV}^2$ ,  
 112 which is the most important region for  $a_\mu^{\text{HLbL}}$ , the only measurement comes from the  
 CELLO experiment with poor accuracy.

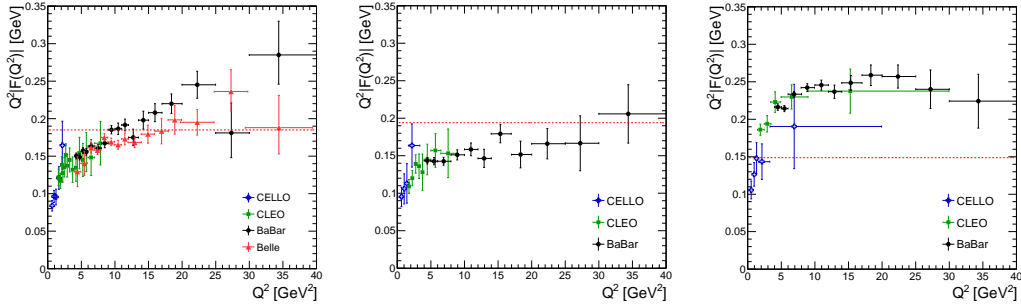


Figure 2: The TFF of  $\pi^0$  (left),  $\eta$  (middle), and  $\eta'$  (right) measured from the CELLO [21], CLEO [22], BaBar [18,19], and Belle [20] experiments.

113

#### 114 4.1 Space-like transition form factor measurements

115 Comparing to the B-factories, the BESIII experiment runs at much lower CM energies,  
 116 thus can measure the TFF in the lower  $Q^2$  region. The data sample collected at the  
 117  $\psi(3770)$  peak has been used to measure the TFFs of the  $\pi^0$ ,  $\eta$ , and  $\eta'$ .

118 In the measurement of the TFF of  $\pi^0$ , the  $\pi^0$  is reconstructed using its  $\gamma\gamma$  final state.  
 119 Events with only one lepton, two to four photons reconstructed in the detector are con-  
 120 sidered as the signal candidates. Using momentum conservation, the untagged lepton is  
 121 required to fly along the beam direction,  $|\cos\theta_{\text{miss}}| \leq 0.99$ . Background events mainly  
 122 come from the radiative Bhabha scattering process, where the hard radiative photon com-  
 123 bined with soft photons forms a fake  $\pi^0$ . These events has been suppressed with conditions  
 124 put on the helicity angle of the  $\pi^0$  candidates ( $|\cos\theta_H| \leq 0.8$ ). A further requirement of  
 125  $\frac{\sqrt{s} - E_{l\pi^0}^* - p_{l\pi^0}^*}{\sqrt{s}} < 0.05$  is applied, where  $E_{l\pi^0}^*$  and  $p_{l\pi^0}^*$  are the sum of the energy and three-  
 126 momentum of the tagged lepton and  $\pi^0$  in the CM frame. This requirement suppresses  
 127 events with large initial state radiation, leading to incorrect reconstruction of  $Q^2$ . The  
 128 background events from charmonium decays with various hadrons in the final states can  
 129 also be removed with this requirement. Events after these selections show a clear  $\pi^0$  peak  
 130 in the  $\gamma\gamma$  invariant mass spectrum, as shown in Fig. 3. In the plots, the red histogram is  
 131 from a signal Monte Carlo (MC) simulation by using EKHARA event generator [24], other  
 132 colored histograms are from background MC simulations. The discrepancy between data  
 133 and MC simulations comes from the missing components in the MC simulations, which  
 134 are the small angle Bhabha scattering events and the  $f_2(1270)$  resonant from  $\gamma\gamma \rightarrow \pi^0\pi^0$   
 135 process. The  $Q^2$  from data and MC simulations are also shown in Fig. 3, the accessible  
 136  $Q^2$  region is  $0.3 \text{ GeV}^2$  to  $3.1 \text{ GeV}^2$ .

137 As the background events distributed smoothly along the  $\gamma\gamma$  invariant mass distribu-  
 138 tion, the number of  $\pi^0$  events is extracted by performing fits to the  $\gamma\gamma$  invariant mass

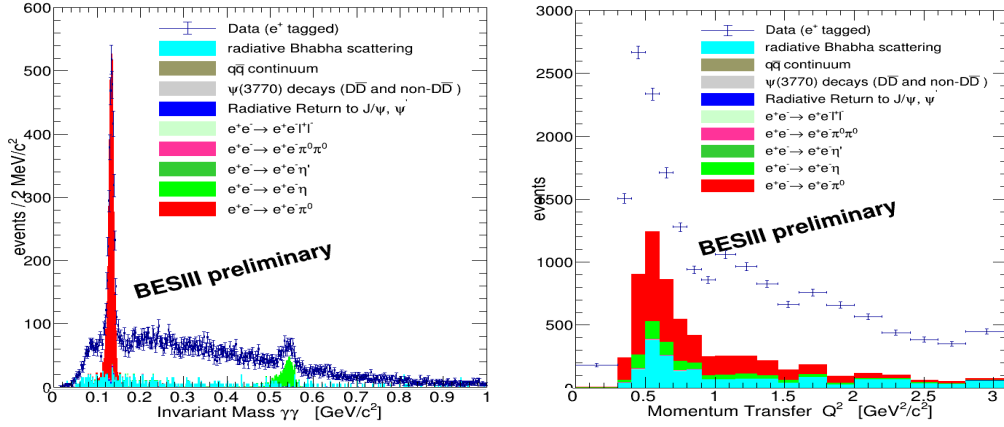


Figure 3: The  $\gamma\gamma$  invariant mass distribution (left) and  $Q^2$  distribution (right) from data and MC simulations. The dot with error bars are data, the red histogram is from signal MC simulation, other colored histograms are from background MC simulations.

139 distributions in bins of  $Q^2$ . The fit is performed with a polynomial function in the  $\pi^0$  side-  
 140 band regions. The fitted curve is extrapolated to the  $\pi^0$  signal region, the events above  
 141 the extrapolated curve in the are considered as signal events. The sideband regions are  
 142 defined as  $[0.070, 0.115]$   $\text{GeV}/c^2$  and  $[0.151, 0.200]$   $\text{GeV}/c^2$ . With the reconstruction effi-  
 143 ciency obtained from the signal MC simulation and the luminosity of the data sample, the  
 144 differential cross section  $d\sigma/dQ^2$  is calculated. The TFF as a function of  $Q^2$  is extracted  
 145 by dividing out the point like cross-section. The result is as shown in Fig. 4. The precision  
 146 in  $Q^2 < 1.5$   $\text{GeV}^2$  is unprecedented, in the  $Q^2$  region above, the precision is compatible  
 to the CLEO [22] result.

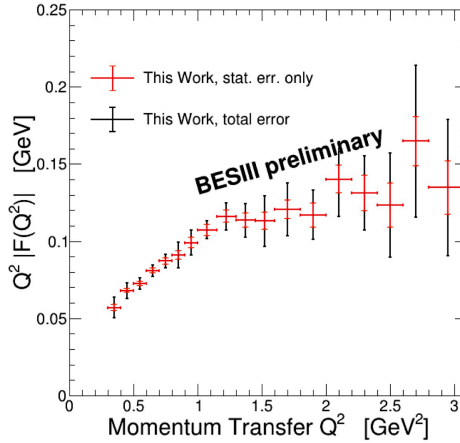


Figure 4: The preliminary result of the  $\pi^0$  TFF from the BESIII experiment.

147  
 148 Comparing the TFF of  $\pi^0$  measured from the BESIII experiment with the model calcu-  
 149 lations [25, 26] and the data-driven approaches [12, 27], the results are shown in Fig. 5. In  
 150 the comparisons, the parameters from the model calculations or data-driven approaches are  
 151 fixed according to the corresponding publications. A  $\chi^2$ , defined as  $\sum_{i=1}^{\text{nbin}=18} \frac{f_i^{\text{exp.}} - f_i^{\text{theo.}}}{\Delta f_i^{\text{exp.}}}$ ,  
 152 is used to obtain the goodness of the agreement. Here  $f_i^{\text{exp.}}$  is the TFF from the BESIII

153 measurement,  $f_i^{\text{theo.}}$  is the value from the theoretical calculations, and  $\Delta f_i^{\text{exp.}}$  is the uncer-  
 154 tainty of the TFF from the BESIII measurement. Among the comparisons to the model  
 155 calculations, the 3–Octet model yields the smallest  $\chi^2$ , ( $\chi^2 = 5.94$ ), 2–Octet model has  
 156 the largest  $\chi^2$  ( $\chi^2 = 24.14$ ). The  $\chi^2$  values for other models are around 9. Considering  
 157 the uncertainty of the measurement, the descriptions from different models are compat-  
 158 ible. The dispersively constructed TFF agrees with the measurement quite well within  
 159 the uncertainties ( $\chi^2 = 11.52$ ). However, the lower edge of the theoretical uncertainty  
 160 band agrees with the measurement better. The description of the TFF using Padé ap-  
 161 proximant is model independent. It uses the TFF from previous measurements in both  
 162 space-like and time-like region to determine the parameters. The comparison with the  
 BESIII measurement shows very good agreement ( $\chi^2 = 5.74$ ).

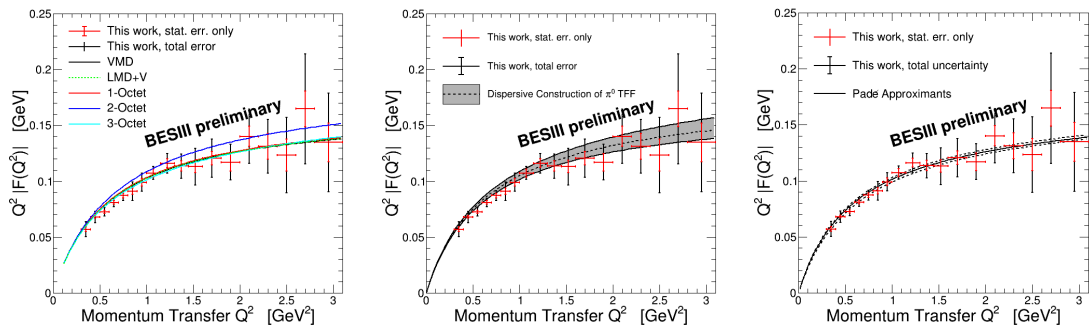


Figure 5: The comparison of the TFF of  $\pi^0$  with model calculations (left), dispersive  
 approach (middle), and Padé approximant (right). The dots with error bars are from the  
 BESIII measurement, the curves with bands are from theoretical calculations.

163 With an analysis strategy similar to that used in the  $\pi^0$  TFF measurement, the TFFs of  
 164  $\eta$  and  $\eta'$  in space-like regime are measured at BESIII experiment as well. The decay modes  
 165 used are  $\eta \rightarrow \pi^+\pi^-\pi^0$  and  $\eta' \rightarrow \pi^+\pi^-\eta$ , respectively. Both  $\pi^0$  and  $\eta$  are reconstructed  
 166 by their decay into  $\gamma\gamma$ . The TFFs can be extracted in the region  $0.3 \leq Q^2$  [GeV $^2$ ]  $\leq 3.5$   
 167 with a precision comparable to the previous results from the CELLO [21] and CLEO [22]  
 168 experiments but in a finer binning of  $Q^2$ . Adding more decay modes and including the  
 169 data samples at CM energies above 4.0 GeV, the precision of these TFF measurements  
 170 can be improved significantly.  
 171

## 172 4.2 Time-like transition form factor measurement of $\eta'$

173 Using  $1.31 \times 10^9$  events taken at the  $J/\psi$  peak, the TFF of  $\eta'$  in time-like region has been  
 174 measured at the BESIII experiment using Dalitz decay process  $\eta' \rightarrow \gamma e^+ e^-$  [28]. It is the  
 175 first measurement of the  $\eta'$  Dalitz decay with an  $e^+ e^-$  pair in the final state.  $864 \pm 36$  signal  
 176 events has been found by fitting to the  $\gamma e^+ e^-$  invariant mass distribution. The branching  
 177 fraction  $\mathcal{B}(\eta' \rightarrow \gamma e^+ e^-)$  has been determined to be  $(4.69 \pm 0.20(\text{stat}) \pm 0.23(\text{sys})) \times$   
 178  $10^{-4}$ . The transition form factor is extracted in eight  $M_{e^+e^-}$  ( $q$ ) bins from 0.1 GeV/ $c^2$  to  
 179 0.8 GeV/ $c^2$ . The square of the TFF is fitted with a single pole parameterization:

$$|F(q^2)|^2 = \frac{\Lambda^2(\Lambda^2 + \gamma^2)}{(\Lambda^2 - q^2)^2 + \Lambda^2\gamma^2}, \quad (1)$$

180 where the parameters  $\Lambda$  and  $\gamma$  correspond to the mass and width of the Breit-Wigner  
 181 shape for the effective contributing vector meson, and  $q$  is the momentum transferred to  
 182 the lepton pair. The fit result is shown in Fig. 6.

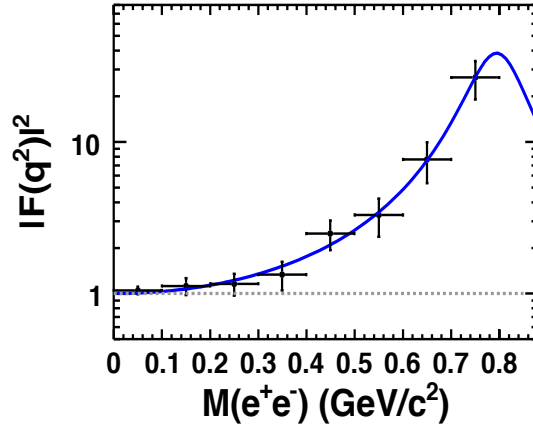


Figure 6: The TFF of  $\eta'$  from the BESIII experiment using Dalitz decay process. The dot with error bars are the measurement and the blue curve is the fit result with the single pole approximation.

183 The  $\Lambda$  and  $\gamma$  values determined from the fit are  $\Lambda_{\eta'} = (0.79 \pm 0.04 \pm 0.02)$  GeV, and  $\gamma_{\eta'} =$   
 184  $(0.13 \pm 0.06 \pm 0.03)$  GeV. The slope of the TFF corresponding to  $(1.60 \pm 0.17 \pm 0.08)$  GeV $^{-2}$   
 185 and agrees within errors with the Vector Meson Dominance predictions and previous  
 186 measurements.

## 187 5 Measurement of $\gamma\gamma^* \rightarrow \pi^+\pi^-$

188 The contributions from meson loops,  $\pi\pi$ ,  $KK$ ,  $\dots$ , are also important ones in the calcu-  
 189 lation of  $a_\mu^{\text{HLbL}}$ . A dispersive analysis for these final states is needed due to the fact that  
 190 the resonances in these final states have finite hadronic decay width, and there are non-  
 191 resonant contributions. Dispersive approaches have been developed [10, 15, 16] recently,  
 192 experimental measurements of  $\gamma^{(*)}\gamma^{(*)} \rightarrow \pi\pi$  and  $\gamma^{(*)}\gamma^{(*)} \rightarrow \pi\eta$  are important test for the  
 193 validity of this approach.

194 The  $\pi^+\pi^-$  final state was measured by the MarkII [29], CELLO [30] and Belle [31]  
 195 experiments, but all in untag method. The cross section as a function of the invariant  
 196 mass of  $\pi^+\pi^-$  ( $W$ ) from these measurements are shown in Fig. 7. The measurements  
 197 from CELLO and Belle measurements start from  $W > 0.8$  GeV/ $c^2$ . The only measure-  
 198 ment at the  $\pi^+\pi^-$  mass threshold region was done by the MarkII experiment with large  
 199 uncertainties and a gap in the region between 0.4 – 0.7 GeV/ $c^2$ .

200 The study at the BESIII experiment is performed with single-tag method. The signal  
 201 events are selected by requiring exact three charged tracks reconstructed in the detector.  
 202 Two of them are identified as pions, the remaining is taken as an electron or positron. The  
 203 dominant background contributions come from  $e^+e^- \rightarrow e^+e^-\mu^+\mu^-$  processes and  $e^+e^- \rightarrow$   
 204  $e^+e^-\pi^+\pi^-$  process (non two-photon process). The  $e^+e^- \rightarrow e^+e^-\mu^+\mu^-$  background events  
 205 is introduced because of  $\pi$ - $\mu$  misidentification. The cross-section is about 6 times larger  
 206 than that of the signal process. This interaction is well-understood from the studies at the  
 207 LEP. MC generators developed for the LEP energy scale [32, 33] have been validated in the  
 208 BESIII energy region. Background contributions remaining after separating pions from  
 209 muons with a multi-variable analysis are subtracted using MC simulations. Backgrounds  
 210 with the same final states as the signal events are mainly from the radiative Bhabha

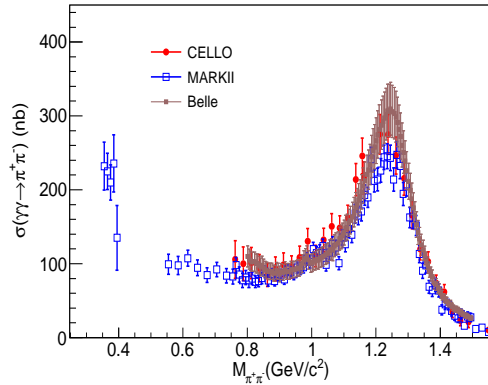


Figure 7: The cross section of  $\gamma\gamma \rightarrow \pi^+\pi^-$  as a function of the invariant mass of  $\pi^+\pi^-$  from the MarkII [29], CELLO [30], and Belle [31] experiments.

211 scattering events, where the radiative photon couples to a vector meson, such as  $\rho$  and  $\omega$   
 212 in the case of  $\pi^+\pi^-$  final state. These events peak in the  $\pi^+\pi^-$  invariant mass spectrum  
 213 and are subtracted by fitting to the  $\pi^+\pi^-$  spectrum in bins of  $Q^2$  and  $\cos\theta^*$ . Here  $\cos\theta^*$   
 214 is the helicity angle of the  $\pi$  in the CM frame of  $\gamma\gamma$ .

215 The remaining events are pure  $\gamma\gamma^* \rightarrow \pi^+\pi^-$  events. From the  $\pi^+\pi^-$  invariant mass  
 216 spectrum, a clear  $f_2(1270)$  signal is observed, as well as an accumulation of events in the  
 217  $f_0(980)$  mass region. The clean signal sample allows a measurement of the differential  
 218 cross-section in bins of  $Q^2$ ,  $W$ , and  $\cos\theta^*$ . This is the first measurement of the two-photon  
 219  $\pi^+\pi^-$  process with a single-tag method. The measurement can provide data points for  
 220  $Q^2$  region from 0.1  $\text{GeV}^2$  to 4.0  $\text{GeV}^2$ ,  $W$  from the  $\pi^+\pi^-$  invariant mass threshold to  
 221 2.0  $\text{GeV}/c^2$ , and a full  $\cos\theta^*$  coverage  $|\cos\theta^*| < 1.0$ .

## 222 6 Conclusion

223 The experimental input for  $a_\mu^{\text{HLbL}}$  calculation, including the TFF of the pseudoscalar  
 224 mesons in both space-like region and time-like region, the helicity amplitude of the  $\pi^+\pi^-$   
 225 final state have been studied at the BESIII experiment. These variables have been mea-  
 226 sured in the most relevant  $Q^2$  region. The TFF of  $\pi^0$  measured at BESIII is unprecedented  
 227 in the  $Q^2$  region from 0.3  $\text{GeV}^2$  to 1.5  $\text{GeV}^2$ . The comparison between the experimen-  
 228 tal result and the theoretical calculations shows good agreement. The first single-tag  
 229  $\gamma\gamma^* \rightarrow \pi^+\pi^-$  analysis can provide measurement in small  $Q^2$  region, as well as in the low  
 230  $\pi^+\pi^-$  invariant mass region down to the threshold with full coverage of  $\cos\theta^*$ . These  
 231 measure are important inputs to the calculation of the HLbL contribution to  $a_\mu$  using a  
 232 dispersive approach.

## 233 References

- 234 [1] G. W. Bennett *et al.* (Muon g-2 Collaboration), *Final report of the E821 muon*  
 235 *anomalous magnetic moment measurement at BNL*, Phys. Rev. D **73**, 072003 (2006),  
 236 doi:10.1103/PhysRevD.73.072003.



- 237 [2] M. Davier, A. Hoecker, B. Malaescu, and Z. Zhang, *Reevaluation of the hadronic*  
238 *vacuum polarisation contributions to the Standard Model predictions of the muon*  
239  *$g - 2$  and  $\alpha(M_Z^2)$  using newest hadronic cross-section data*, Eur. Phys. J. C **77**, 827  
240 (2017), doi:10.1140/epjc/s10052-017-5161-6.
- 241 [3] A. Keshavarzi, D. Nomura, and T. Teubner, *Muon  $g-2$  and  $\alpha(M_Z^2)$ : A new data-based*  
242 *analysis*, Phys. Rev. D **97**, 114025 (2018), doi:10.1103/PhysRevD.97.114025.
- 243 [4] F. Jegerlehner, *Muon  $g - 2$  theory: The hadronic part*, Eur. Phys. J. Web Conf. **166**,  
244 00022 (2018), doi:10.1051/epjconf/201816600022.
- 245 [5] <http://muon-g-2.fnal.gov>.
- 246 [6] <http://g-2.kek.jp/portal/index.html>.
- 247 [7] T. Aoyama, M. Hayakawa, T. Kinoshita, and M. Nio, *Complete tenth-order*  
248 *QED contribution of the muon  $g - 2$* , Phys. Rev. Lett. **109**, 111808 (2012),  
249 doi:10.1103/PhysRevLett.109.111808.
- 250 [8] C. Gnendiger, D. Stöckinger, and H. Stöckinger-Kim, *The electroweak contributions*  
251 *to  $(g - 2)_\mu$  after the Higgs-boson mass measurement*, Phys. Rev. D **88**, 053005 (2013),  
252 doi:10.1103/PhysRevD.88.053005.
- 253 [9] M. Hoferichter, B. Kubis, S. Leupold, F. Niecknig, and S. P. Schneider, *Disper-*  
254 *sive analysis of the pion transition form factor*, Eur. Phys. J. C **74**, 3180 (2014),  
255 doi:10.1140/epjc/s10052-014-3180-0.
- 256 [10] G. Colangelo, M. Hoferichter, M. Procura, and P. Stoffer, *Dispersive approach*  
257 *to hadronic light-by-light scattering*, J. High Energy Phys. **09**, 091 (2014),  
258 doi:10.1007/JHEP09(2014)091.
- 259 [11] G. Colangelo, M. Hoferichter, B. Kubis, M. Procura, and P. Stoffer, *Towards a data-*  
260 *driven analysis of hadronic light-by-light scattering*, Phys. Lett. B **738**, 6 (2014),  
261 doi:10.1016/j.physletb.2014.09.021.
- 262 [12] M. Hoferichter, B. Hoid, B. Kubis, S. Leupold, and S. P. Schneider, *Pion-Pole contri-*  
263 *bution to hadronic light-by-light scattering in the anomalous magnetic moment of the*  
264 *muon*, Phys. Rev. Lett. **121**, 112002 (2018), doi:10.1103/PhysRevLett.121.112002.
- 265 [13] M. Hoferichter, B. Hoid, B. Kubis, S. Leupold, and S. P. Schneider, *Dispersion relation*  
266 *for hadronic light-by-light scattering: pion pole*, J. High Energy Phys. **10**, 141 (2018),  
267 doi:10.1007/JHEP10(2018)141.
- 268 [14] V. Pauk and M. Vanderhaeghen, *Anomalous magnetic moment of the muon in a dis-*  
269 *persive approach*, Phys. Rev. D **90**, 113012 (2014), doi:10.1103/PhysRevD.90.113012.
- 270 [15] I. Danilkin and M. Vanderhaeghen, *Dispersive analysis of the  $\gamma\gamma^* \rightarrow \pi^+\pi^-$  process*,  
271 <https://arxiv.org/pdf/1810.03669.pdf>.
- 272 [16] O. Deineka, I. Danilkin, and M. Vanderhaeghen, *Theoretical analysis of the  $\gamma\gamma^{(*)} \rightarrow$*   
273  *$\pi^0\eta$  process*, <https://arxiv.org/pdf/1808.04117.pdf>.
- 274 [17] Ablikim M *et al.* (BESIII Collaboration), *Design and construction of the BESIII*  
275 *detector*, Nucl. Instrum. Meth. A **614**, 345 (2010), doi:10.1016/j.nima.2009.12.050.
- 276 [18] B. Aubert *et al.* (BaBar Collaboration), *Measurement of the  $\gamma\gamma^* \rightarrow \pi^0$  transition*  
277 *form factor*, Phys. Rev. D **80**, 052002 (2009), doi:10.1103/PhysRevD.80.052002.

- 278 [19] P. del Amo Sanchez *et al.* (BaBar Collaboration), *Measurement of the  $\gamma\gamma^* \rightarrow$*   
279  *$\eta$  and  $\gamma\gamma^* \rightarrow \eta'$  transition form factors*, Phys. Rev. D **84**, 052001 (2011),  
280 doi:10.1103/PhysRevD.84.052001.
- 281 [20] S. Uehara *et al.* Belle Collaboration, *Measurement of  $\gamma\gamma^* \rightarrow \pi^0$  transition form factor*  
282 *at Belle*, Phys. Rev. D **86**, 092007 (2012), doi:10.1103/PhysRevD.86.092007.
- 283 [21] H. J. Behrend *et al.* (CELLO Collaboration), *A measurement of the  $\pi^0$ ,  $\eta$ , and  $\eta'$  elec-*  
284 *tromagnetic form factors*, Z. Phys. C **49**, 401-409 (1991), doi:10.1007/BF01549692.
- 285 [22] J. Gronberg *et al.* (CLEO Collaboration), *Measurements of the meson-photon tran-*  
286 *sition form factors of light pseudoscalar mesons at large momentum transfer*, Phys.  
287 Rev. D **57**, 33 (1998), doi:10.1103/PhysRevD.57.33.
- 288 [23] A. Nyffeler, *Precision of a data-driven estimate of hadronic light-by-light scattering*  
289 *in the muon  $g - 2$ : Pseudoscalar-pole contribution*, Phys. Rev. D **94**, 053006 (2016),  
290 doi:10.1103/PhysRevD.94.053006.
- 291 [24] H. Czyz, S. Ivashyn, A. Korchin, and O. Shekhovtsova, *Two-photon form factors of*  
292 *the  $\pi^0$ ,  $\eta$ , and  $\eta'$  mesons in the chiral theory with resonances*, Phys. Rev. D **85**,  
293 094010 (2012), doi:10.1103/PhysRevD.85.094010; H. Czyz and P. Kiszka, *EKHARA*  
294 *3.0: an update of the EKHARA monte carlo event generator*, [https://arxiv.org/](https://arxiv.org/pdf/1805.07756.pdf)  
295 [pdf/1805.07756.pdf](https://arxiv.org/pdf/1805.07756.pdf).
- 296 [25] M. Knecht and A. nyffeler, *Hadronic light-by-light corrections to the muon*  
297  *$g - 2$ : The poin-pole contribution*, Phys. Rev. D **65**, 073034 (2002),  
298 doi:10.1103/PhysRevD.65.073034.
- 299 [26] H. Czyz, P. Kiszka, and S. Tracz, *Modeling interactions of photons*  
300 *with pseudoscalar and vector meacons*, Phys. Rev. D **97**, 016006 (2018),  
301 doi:10.1103/PhysRevD.97.016006.
- 302 [27] P. Masjuan,  *$\gamma\gamma^* \rightarrow \pi^0$  transition form factor at low energies from a model-independent*  
303 *approach*, Phys. Rev. D **86**, 094021 (2012), doi:10.1103/PhysRevD.86.094021.
- 304 [28] M. Ablikim *et al.* (BESIII Collaboration), *Observation of the Dalitz decay  $\eta' \rightarrow \gamma e^+ e^-$* ,  
305 Phys. Rev. D **92**, 012001 (2015), doi:10.1103/PhysRevD.92.012001.
- 306 [29] J. Boyer *et al.*, *Two-photon production of pion pairs*, Phys. Rev. D **42**, 1350 (1990),  
307 doi:10.1103/PhysRevD.42.1350.
- 308 [30] H. Behrend *et al.* (CELLO Collaboration), *An experimental study of the process*  
309  *$\gamma\gamma \rightarrow \pi^+ \pi^-$* , Z. Phys. C **56**, 381-390 (1992), doi:10.1007/BF01565945.
- 310 [31] T. Mori *et al.* (Belle Collaboration), *High statistics study of the  $f_0(980)$  res-*  
311 *onance in  $\gamma\gamma \rightarrow \pi^+ \pi^-$  production*, Phys. Rev. D **75**, 051101(R) (2007),  
312 doi:10.1103/PhysRevD.75.051101.
- 313 [32] F. A. Berends, P. H. Daverveldt, and R. Kleiss, *Monte Carlo simulation of two-*  
314 *photon processes: II: complete lowest order calculations for four-lepton production*  
315 *processes in electron-positron collisions*, Comput. Phys. Commun. **40**, 285-307 (1986),  
316 doi:10.1016/0010-4655(86)90115-3.
- 317 [33] F. A. Berends, P. H. Daverveldt, and R. Kleiss, *Monte Carlo simulation of two-photon*  
318 *processes: I: radiative corrections to multiperipheral  $e^+ e^- \mu^+ \mu^-$  production*, Comput.  
319 Phys. Commun. **40**, 271-284 (1986), doi:10.1016/0010-4655(86)90114-1.